GRAPHENE

Imaging resonant dissipation from individual atomic defects in graphene

Dorri Halbertal,[1]* Moshe Ben Shalom,[2]* Aviram Uri,[1] Kousik Bagani,[1]
Alexander Y. Meltzer,[1] Ido Marcus,[1] Yuri Myasoedov,[1] John Birkbeck,[2]
Leonid S. Levitov,[3] Andre K. Geim,[2] Eli Zeldov[1]*

Conversion of electric current into heat involves microscopic processes that operate on
nanometer length scales and release minute amounts of power. Although central to
our understanding of the electrical properties of materials, individual mediators of energy
dissipation have so far eluded direct observation. Using scanning nanothermometry
with submicrokelvin sensitivity, we visualized and controlled phonon emission from individual
atomic-scale defects in graphene. The inferred electron-phonon "cooling power spectrum"
exhibits sharp peaks when the Fermi level comes into resonance with electronic quasi-bound
states at such defects. Rare in the bulk but abundant at graphene's edges, switchable
atomic-scale phonon emitters provide the dominant dissipation mechanism. Our work offers
insights for addressing key materials challenges in modern electronics and enables control
of dissipation at the nanoscale.

Understanding the microscopic mechanisms of momentum and energy dissipation is a central problem in fields ranging from condensed matter to particle physics. It is also of keen interest to researchers designing new approaches to handle, convert, and use energy. Dissipation pathways are particularly intriguing in ultrapure materials, such as graphene (1), because of tight restrictions on the phase space for electron-phonon scattering (2–4). Furthermore, in condensed matter physics, we are interested in processes concealed within materials. This lack of access, along with the fact that the power released in such processes is very small, poses a key challenge for experimentally probing dissipation at the nanoscale. We used a recently developed ultrasensitive scanning nanothermometer with submicrokelvin sensitivity (5), achieved with a superconducting quantum interference device (SQUID) placed on an extremely sharp tip (SQUID-on-tip, or SOT), to probe these subtle effects in high-mobility graphene. Owing to its exceptional cleanliness and the two-dimensional nature of its electrons and phonons (1), graphene is an excellent platform to study electron-phonon relaxation.

Our measurements were performed on exfoliated graphene encapsulated between hexagonal boron nitride (hBN). Charge carriers were injected into a micron-scale "electron chamber" by applying electrical current through narrow constrictions [Fig. 1, A and B, and section 1 of (6)]. Transport measurements in such samples routinely show ballistic signatures over a wide range of temperatures and carrier densities (7–9). Our SQUID-on-tip (10) acts as an extremely sensitive thermometer (tSOT) (5) with an effective diameter of 33 nm and thermal sensitivity of 510 nK/Hz$^{1/2}$ at 4.2 K, and it provides a map of the local temperature variations $\delta T(x, y)$ upon scanning at a height h of 10 to 40 nm above the sample surface (as specified for each measurement). The tip is mounted on a quartz tuning fork (11), which allows the tSOT to vibrate parallel to the sample surface with a controlled amplitude x_{ac} = 2.7 nm at a frequency of ~37 kHz [sections 2 and 3 of (6)]. The resulting ac signal, $T_{ac}(x, y) = x_{ac}\partial\delta T(x, y)/\partial x$, renders higher-sensitivity imaging (Fig. 1C) by avoiding the low-frequency $1/f$ noise of the tSOT. We control the carrier density in graphene globally by a back-gate bias V_{bg} to the Si/SiO$_2$ substrate and locally by applying a tip potential V_{tg} to the tSOT (Fig. 1A). Description of sample fabrication and thermal imaging is provided in (6).

Figure 1C shows the thermal signal $T_{ac}(x, y)$ measured while applying a fixed current I_{dc} = 3 μA through two of the constrictions, as shown in Fig. 1B. The image reveals a complex array of fine rings along the edges of the heterostructure (5). In addition, three isolated rings are observed in the bulk of graphene, labeled A, B, and C. The bulk rings are rare and have comparable diameters, in sharp contrast to the rings at the edges, which are dense and display widely varying sizes (movies S1 and S2). We show below that the rings mark dissipation from single atomic defects positioned at their centers.

Electron-phonon cooling pathways in graphene are particularly interesting for several reasons. Owing to the exceptional stiffness of the carbon bonds, scattering by optical phonons in graphene is inefficient below room temperature. Moreover, the small size of the electron's Fermi surface re-stricts the phase volume for scattering by acoustic phonons, blocking the intrinsic electron-lattice relaxation pathway (2–4). However, theory predicts that disorder can substantially ease the electron-phonon scattering (4). Our key finding is that hot electrons, generated by the applied current, dissipate their energy through a very specific disorder-induced mechanism: resonant inelastic scattering by local electronic resonances caused by individual defects. Each such localized state (LS) mediates cooling through resonant electron scattering, creating an atomic-scale thermal link between the electronic bath, at an effective hot-electron temperature T_e, and the phonon bath, at a base temperature T_p [section 4 of (6)]. To characterize this thermal link, we define the electron-phonon heat conductivity of a defect, $\kappa_{ep}(\varepsilon)$, which describes the power transferred between the baths, $P_{ep}(\varepsilon) = \kappa_{ep}(\varepsilon)\Delta T$ (where $\Delta T = T_e - T_p$ and ε is the energy relative to the Dirac point). The resulting "cooling power spectrum" $P_{ep}(\varepsilon)$ (CPS)—the fundamental quantity accessed in our experiment through local temperature increase $\delta T(\varepsilon) \propto P_{ep}(\varepsilon)$—is found to peak sharply when the Fermi level E_F is aligned with the quasi-bound LS resonant energy E_{LS}.

Our analysis [section 4 of (6)] of the observed resonances suggests that they originate from quasi-bound states arising at a carbon vacancy or adatom bonded to a single C atom when its sp^2 orbital transforms to an sp^3 state (12–15). Such defects are known to produce sharp electronic resonances at energies near the Dirac point (16, 17). Although these defects have been extensively investigated by means of ab initio calculations and scanning tunneling microscopy (STM) (12–19), their prominent role in dissipation has not been anticipated by previous work. The defect-induced CPS originates from the part of the local density of electronic states that mediates electron-phonon coupling [EP-LDOS, $D_{ep}(\varepsilon)$]—a hitherto inaccessible quantity—convoluted with the electron and phonon Fermi and Bose energy distribution functions, respectively [section 4 of (6)]. Our measurements and analysis indicate that the spectral width of $D_{ep}(\varepsilon)$ is much greater than the thermal broadening, in which case the CPS can be approximated as $P_{ep}(\varepsilon) \propto D_{ep}(\varepsilon)$ [section 4 of (6)]. This quantity can be probed experimentally, as illustrated schematically in Fig. 2, A to C. By parking the tSOT above the defect and varying V_{tg}, we can induce local band bending that shifts $D_{ep}(\varepsilon)$ with respect to E_F [Fig. 3A and section 6 of (6)]. The resulting variation in the measured temperature, $\delta T(V_{tg})$, provides a spectroscopic measurement of $P_{ep}(\varepsilon) \propto D_{ep}(\varepsilon)$ (Fig. 2B). Additional information can be obtained by tuning E_F by the back-gate V_{bg}, yielding resonant peaks in $D_{ep}(\varepsilon)$ aligned as diagonal lines in the $\delta T(V_{tg}, V_{bg})$ map (Fig. 2C). Importantly, in this configuration, phonon emission can be turned on and off by applying a potential on the tSOT tip, demonstrating control of nonequilibrium dynamics and probing them at the nanoscale.

The experimental $\delta T(V_{tg}, V_{bg})$ map of defect C (Fig. 2D) displays, in agreement with the discussion above, a sharp resonance (Fig. 2E) along a single diagonal line, which passes close

[1]Department of Condensed Matter Physics, Weizmann Institute of Science, Rehovot 7610001, Israel. [2]National Graphene Institute and School of Physics and Astronomy, The University of Manchester, Manchester M13 9PL, UK. [3]Department of Physics, Massachusetts Institute of Technology, Cambridge, MA 02139, USA.
*Corresponding author. Email: dorri.halbertal@weizmann.ac.il (D.H.); moshebs@tauex.tau.ac.il (M.B.S.); eli.zeldov@weizmann.ac.il (E.Z.)
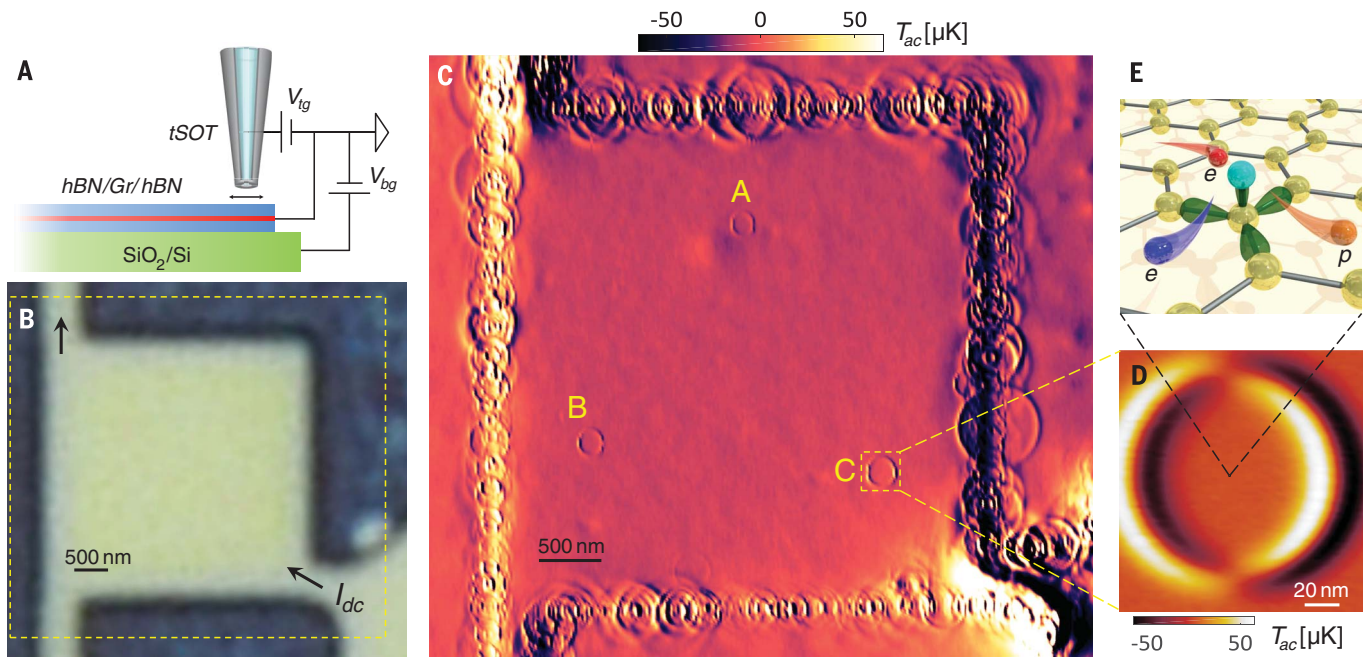
Fig. 1. Observing individual dissipation sources in a graphene heterostructure. (**A**) Schematic side view of the measurement setup with the hBN-graphene-hBN heterostructure and SQUID-on-tip nanothermometer (tSOT). (**B**) Optical image of the device patterned into a square chamber (bright; 4 μm × 4 μm). A fixed current I_{dc} = 3 μA is driven through the connecting constrictions (arrows). (**C**) Scanning ac nanothermometry $T_{ac}(x, y)$ of the area outlined in (B) at V_{bg} = −2 V, V_{tg} = 9 V, and 4.2 K. The tSOT scans the sample while oscillating with amplitude x_{ac} = 2.7 nm at 12° to the x axis. Scan area, 5.5 μm × 5 μm; pixel size, 18 nm; scan speed, 20 ms per pixel; height h = 20 nm; I_{dc} = 3 μA. The sharp rings (marked A, B, and C) uncover three isolated sources of dissipation in the bulk of graphene, in addition to a dense array of resonances along the graphene edges. (**D**) Zoomed-in view of defect C at V_{tg} = 5 V. Scan area, 140 nm × 150 nm; pixel size, 1.9 nm; scan speed, 20 ms per pixel; h = 20 nm; I_{dc} = 3 μA. (**E**) Illustration of an atomic defect in graphene that creates a localized resonant dissipative state at the center of the ring (D), which in turn mediates inelastic scattering of an impinging electron (red) into a phonon (orange) and a lower-energy electron (blue). The defect, forming an sp^3 orbital (green), can arise from a carbon vacancy, adatom, or admolecule.
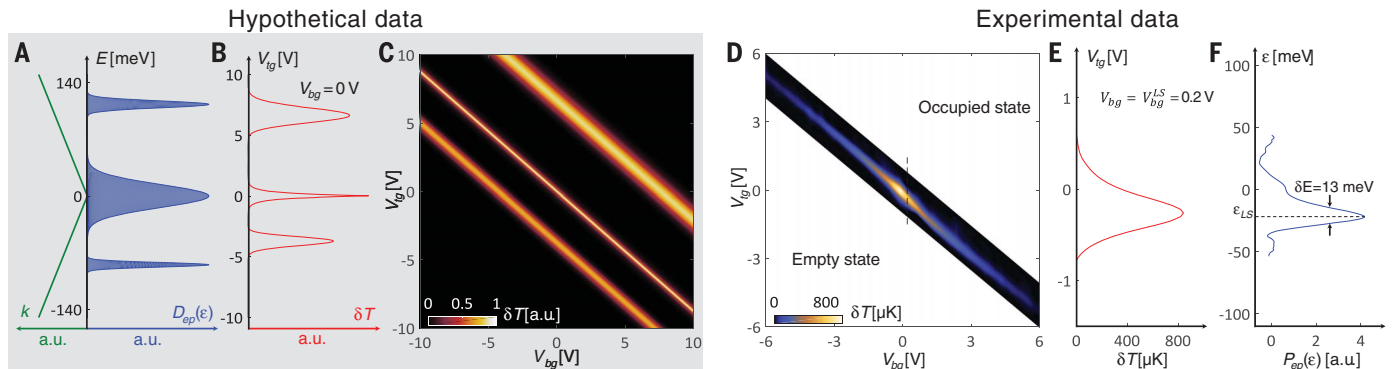

Fig. 2. Thermal nanospectroscopy of dissipative localized states. (**A**) Schematic example of a spectrum of EP-LDOS [$D_{ep}(\varepsilon)$, blue] and the graphene Dirac dispersion relation (green). a.u., arbitrary units; k, wave number. (**B**) Temperature variation $\delta T(V_{tg})$ as would be measured above the defect versus tip potential V_{tg}, providing nanoscale spectroscopy of the cooling power spectrum $P_{ep}(\varepsilon)$ by tip-induced band bending. (**C**) The expected $\delta T(V_{bg}, V_{tg})$, showing diagonal resonance lines that map the peaks in $D_{ep}(\varepsilon)$ [calculation details are given in section 6 of (6)]. (**D**) The experimental $\delta T(V_{bg}, V_{tg})$, measured by the tSOT at h = 10 nm above the center of defect C in the presence of I_{dc} = 3 μA, revealing a single resonance dissipation line (data were not taken for the white portion of the plane in this measurement). The signal was obtained through integration of T_{ac}^{tg} over V_{tg} [section 2 of (6)]. (**E**) A zoomed-in line cut of $\delta T(V_{tg})$ along the dashed line in (D) at $V_{bg} = V_{bg}^{LS}$ = 0.2 V. (**F**) The cooling power spectrum $P_{ep}(\varepsilon) \propto D_{ep}(\varepsilon)$, derived from the measurement of the resonant dissipation ring [section 9 of (6)], showing a single sharp peak near the Dirac point at ε_{LS} = −22 meV.

to the origin in the V_{tg}-V_{bg} plane. This resonance is caused by the presence of a LS with a narrow single peak in $D_{ep}(\varepsilon)$ (Fig. 2F) close to the Dirac energy [section 8 of (6)]. Such LSs give rise to the sharp thermal rings observed in Fig. 1C as

follows. For the LS to cause inelastic electron scattering, its energy level E_{LS} has to be aligned with the energy of the impinging electrons, $E_e \cong E_F$ (the global Fermi energy). For a given tip potential V_{tg}, this resonant condition occurs when

the tip is located at a distance R from a LS [Fig. 3A, movie S3, and section 6 of (6)]. As a result, each LS displays a sharp peak in $\delta T(x, y)$ and $T_{ac}(x, y)$ along a ring of radius R (Fig. 3B), describing the ring formations in Figs. 1C and 3C.
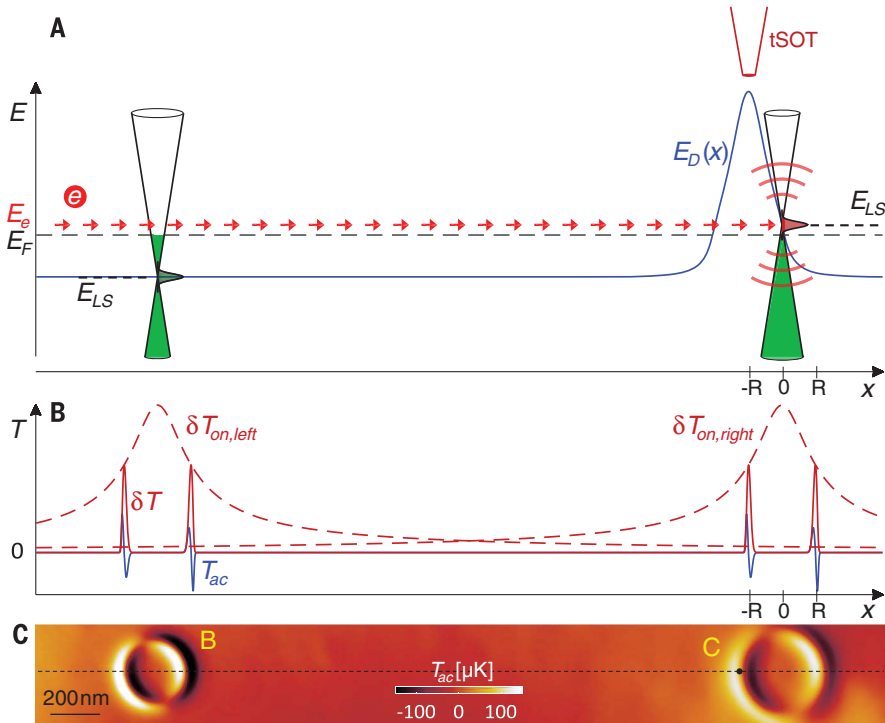
Fig. 3. Origin of the resonant ring structures. (**A**) Schematic description of the system's energy levels corresponding to tip position marked by the black point in (C): two localized states with a peak in EP-LDOS at E_{LS} pinned to Dirac energy E_D. The tip potential V_{tg} induces band bending, resulting in the calculated position-dependent $E_D(x)$ (blue). The left LS is off-resonance, whereas the tSOT positioned at $x = -R$ brings the right LS into resonance for inelastic scattering of electrons injected at energy E_e (red arrows). The result is a point source of phonon emission (red arcs). The Fermi energy E_F (gray dashed line) is determined by the back-gate voltage V_{bg}. (**B**) Red dashed lines, schematic temperature profiles resulting from ballistic two-dimensional phonon emission from LS at resonant conditions, $\delta T_{on}(x) \propto \left[1 + (x/\ell)^2\right]^{-1/2}$, with $\ell = 100$ nm [section 5.2 of (6)]. Red solid line, calculated temperature variation $\delta T(x)$ measured by the scanning tSOT that brings the LS into resonance at a distance $\pm R$ from each defect. Blue solid line, calculated $T_{ac}(x) = x_{ac}\partial\delta T(x)/\partial x$, as would be measured by the tSOT vibrating with amplitude x_{ac} parallel to the surface [section 6 of (6)]. (**C**) $T_{ac}(x, y)$ measured in the central region of Fig. 1C, showing dissipation rings around defects B and C. The dashed line describes the scan direction depicted in (A). Scan area, 3.5 μm × 0.4 μm; pixel size, 8 nm; scan speed, 20 ms per pixel; $h = 20$ nm; $V_{bg} = -0.3$ V; $V_{tg} = 5.5$ V; $I_{dc} = 6$ μA; $x_{ac} = 2.7$ nm directed at 18° to the x axis.

The variable tip and back-gate potentials also provide the spectroscopic means to extract the energy level and the CPS of the LS. By repeatedly scanning the tSOT along the line crossing the defect and incrementing V_{bg}, a bell-shaped resonance trace is obtained (Fig. 4A). The shape and polarity of the trace confirm the electrostatic picture described above [Fig. 4, A to C; section 7 of (6); and movies S5 and S6], and its asymptotic value V_{bg}^{LS} describes the energy level E_{LS} of the LS. Similar information can be obtained by sweeping V_{tg} at various values of V_{bg} [section 7 of (6) and movies S4 and S7].

Our spectroscopic analysis of bulk LSs leads to the following conclusions: (i) The LS energy resides slightly below the Dirac point ($\varepsilon_{LS} = E_{LS} - E_D \cong -22$ meV), as derived from the analysis of the resonance lines [section 8 of (6)]. (ii) The spectral width of the CPS [$P_{ep}(\varepsilon)$] is about 13 meV [Fig. 2F and section 9 of (6)]. (iii) No additional LS energy levels are observed at least 180 meV above and below E_{LS}. If present, additional concentric rings and bell-shaped traces would have formed; however, these are absent for the entire V_{bg} and V_{tg} applied range of ±10 V [section 7 of (6)]. (iv) This level spacing puts an upper bound on the spatial extent of the LS of less than 2 nm, based on a charging energy calculation [section 7 of (6)]. (v) The sharp energy level and nanometer spatial extent of the LS closely resemble the characteristic features of atomic defects in graphene derived from ab initio calculations (14) and observed using STM (16, 17), in contrast to more extended non-resonant "puddles" originating from disordered substrate potential (20, 21). (vi) The resonant character of the defects and the energy level close to the Dirac point are consistent with the sp3 band vacancy model. In particular, vacancies and monovalent adatoms are known to form LSs at energies comparable to our measured values (14, 16) [section 4 of (6)] and thus are strong candidates for the observed bulk defects. (vii) The bulk defects are extremely rare (we found only seven such defects in total in 13 samples with a total area of 3500 μm²), corresponding to an estimated average areal density of 2×10^5 cm^{-2} or volume concentration of 5×10^{-5} parts per million if originating from the parent graphite. Their spectral properties appear to be the same within our experimental resolution [section 8 of (6)], pointing to a common chemical or structural origin.

These conclusions are reinforced by examining the LSs along the edges of graphene, which display spectroscopic features very similar to those of the bulk defects, but with some notable differences. Shown in Fig. 4, D and E, are tSOT line scans along the bottom edge of the sample that cross through numerous LSs, taken while increasing V_{bg} (movies S6 and S7). Each LS is visible as a bell-shaped trace, similar to the ones in Fig. 4, A to C, indicating the same microscopic origin of different LSs. In contrast to LSs in the bulk, the edge LSs are extremely dense, with some adjacent states only about 1 nm apart (fig. S15E). This puts an additional bound on their spatial extent [section 10 of (6)]. We ascribe their origin to the carbon dangling bonds near the edge with high affinity to adatoms and molecules, giving rise to resonance states formed by the resulting sp3 vacancies (12–15). Notably, unlike the LSs in the bulk, the edge LSs display large variations in E_{LS} values, manifested in Fig. 4, D and E, by the vertical spread of the bell-shaped traces over the entire V_{bg} range of 20 V. This translates into a 260-meV spread in E_{LS}, limited by our bias range. We are able to resolve states that are less than 2 nm apart but differ in their E_{LS} by as much as 160 meV [section 10 of (6)]. Such large energy-level variation may arise from the atomic defects at graphene edges having more diverse chemical origins than the native bulk defects. An alternative explanation is Coulomb interaction between the charged defects. Charging a LS by one electron would shift the energy of a neighboring LS at a distance of 2 nm by ~240 meV [section 7 of (6)], consistent with our observations.

The above results suggest that hot electrons lose most of their energy to phonons at the edges of graphene. To verify this conjecture, we measured the bare $\delta T(x, y)$ in the absence of tSOT electrostatic influence [$V_{tg} = V_{tg}^{FB}$ at a flat-band condition; section 5 of (6)]. Measurement of sample 2 (Fig. 4, F and G) revealed a higher temperature along the sample edges relative to the temperature in the sample bulk. Together with numerical simulations [section 5 of (6)], this finding implies that the LSs along the graphene edges are the dominant source of dissipation at all doping levels reachable in our experiment. Therefore, the excess phonons, corresponding to the overall temperature rise, are not generated locally in the graphene bulk. Instead, the phonons are predominantly emitted through inelastic electron scattering by those LSs at graphene edges that are at resonance at a given V_{bg} value [section 5
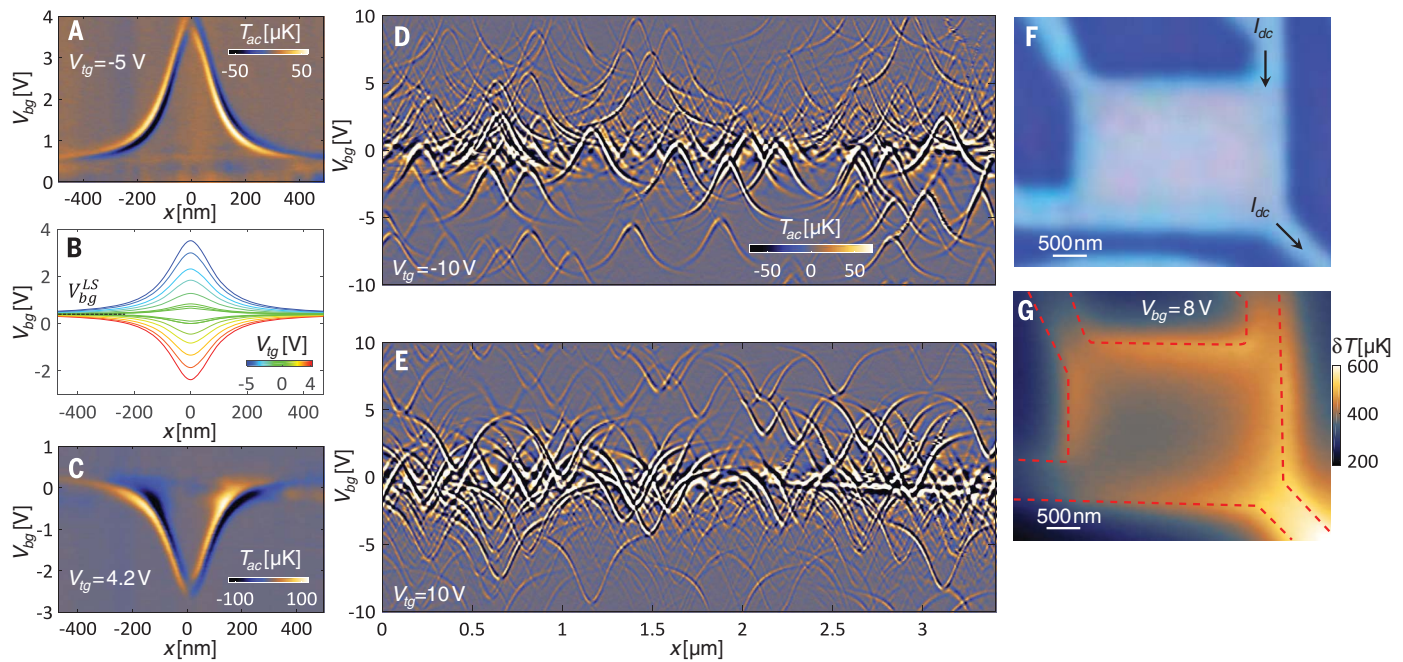
Fig. 4. Thermal spectroscopy of individual bulk and edge localized states. (**A**) Map of $T_{ac}(x)$ line scans through defect C while varying V_{bg} at $V_{tg} = -5$ V, showing the bell-shaped resonance trace. (**B**) Resonance traces for various values of V_{tg} that switch their polarity at V_{bg}^{LS}. (**C**) Resonance trace as in (A) at $V_{tg} = 4.2$ V. In (A) to (C), $h = 20$ nm; pixel width, 5 nm; pixel height, 30 mV; scan speed, 20 ms per pixel; $x_{ac} = 2.7$ nm; $I_{dc} = 3$ µA; a linear fit was subtracted from each line to emphasize the resonance traces (fig. S11 and movie S5 show raw images). (**D** and **E**) Maps of $T_{ac}(x)$ line scans along the bottom edge of the square graphene sample in Fig. 1C at $V_{tg} = -10$ V (D) and 10 V (E). Each bell-shaped trace originates from a single dissipative atomic defect. In (D) and (E), $h = 20$ nm; pixel width, 4 nm; pixel height, 100 mV; scan speed, 60 ms per pixel; $x_{ac} = 2.7$ nm; $I_{dc} = 3$ µA. (**F**) Optical image of sample 2, with a patterned hBN/graphene/hBN heterostructure (bright) on a SiO$_2$ substrate (dark) and dc current I_{dc} chopped at 35.5 Hz with a root mean square value of 1 µA, applied as indicated by the arrows. (**G**) Thermal image of $\delta T(x, y)$ revealing dissipation along the graphene edges. Scan area, 4.7 µm × 3.7 µm; pixel size, 50 nm; scan speed, 200 ms per pixel; $h = 20$ nm; $V_{bg} = 8$ V; $V_{tg} = 0.85$ V, corresponding to V_{tg}^{FB} (flat-band condition) at this V_{bg}.

of (6)]. The observed atomic-scale resonant LSs thus emerge as the leading mechanism of dissipation in clean graphene, each acting as a pointlike source emitting phonons that then propagate ballistically throughout the entire sample.

The observation of sharply localized resonant states and their role in dissipation should have considerable implications for understanding the thermal (22), magnetic (12, 16, 23), chemical (24), and transport (25–28) properties of graphene. These states are distinct from the extended edge states anticipated for crystalline graphene edges (23). Further, resonant dissipation is completely different from the conventional nonresonant picture of electron-phonon coupling (2–4), posing interesting questions for future experimental and theoretical work. This dissipation mechanism may affect the edge transport characteristics (29–31) and explain previous observations of the mean free path being limited by the device size in state-of-the-art encapsulated graphene (7–9). The resonance states, localized at the edge and in the bulk, thus emerge as a key factor governing the dissipation and possibly limiting the carrier mobility in pure graphene.

REFERENCES AND NOTES

1. A. H. Castro Neto, F. Guinea, N. M. R. Peres, K. S. Novoselov, A. K. Geim, *Rev. Mod. Phys.* **81**, 109–162 (2009).
2. R. Bistritzer, A. H. MacDonald, *Phys. Rev. Lett.* **102**, 206410 (2009).
3. W. K. Tse, S. Das Sarma, *Phys. Rev. B* **79**, 235406 (2009).
4. J. C. W. Song, M. Y. Reizer, L. S. Levitov, *Phys. Rev. Lett.* **109**, 106602 (2012).
5. D. Halbertal et al., *Nature* **539**, 407–410 (2016).
6. Materials and methods are available as supplementary materials.
7. C. R. Dean et al., *Nat. Nanotechnol.* **5**, 722–726 (2010).
8. A. S. Mayorov et al., *Nano Lett.* **11**, 2396–2399 (2011).
9. D. A. Bandurin et al., *Science* **351**, 1055–1058 (2016).
10. D. Vasyukov et al., *Nat. Nanotechnol.* **8**, 639–644 (2013).
11. A. Finkler et al., *Rev. Sci. Instrum.* **83**, 073702 (2012).
12. V. M. Pereira, F. Guinea, J. M. B. Lopes dos Santos, N. M. R. Peres, A. H. Castro Neto, *Phys. Rev. Lett.* **96**, 036801 (2006).
13. D. W. Boukhvalov, M. I. Katsnelson, A. I. Lichtenstein, *Phys. Rev. B* **77**, 035427 (2008).
14. T. O. Wehling, M. I. Katsnelson, A. I. Lichtenstein, *Phys. Rev. B* **80**, 085428 (2009).
15. A. V. Shytov, D. A. Abanin, L. S. Levitov, *Phys. Rev. Lett.* **103**, 016806 (2009).
16. H. González-Herrero et al., *Science* **352**, 437–441 (2016).
17. J. Mao et al., *Nat. Phys.* **12**, 545–549 (2016).
18. Z. H. Ni et al., *Nano Lett.* **10**, 3868–3872 (2010).
19. M. Titov, P. M. Ostrovsky, I. V. Gornyi, A. Schuessler, A. D. Mirlin, *Phys. Rev. Lett.* **104**, 076802 (2010).
20. D. Wong et al., *Nat. Nanotechnol.* **10**, 949–953 (2015).
21. J. Martin et al., *Nat. Phys.* **4**, 144–148 (2008).
22. F. Menges, H. Riel, A. Stemmer, C. Dimitrakopoulos, B. Gotsmann, *Phys. Rev. Lett.* **111**, 205901 (2013).
23. C. Tao et al., *Nat. Phys.* **7**, 616–620 (2011).
24. J. Dauber, B. Terres, C. Volk, S. Trellenkamp, C. Stampfer, *Appl. Phys. Lett.* **104**, 083105 (2014).
25. D. Bischoff et al., *Appl. Phys. Rev.* **2**, 031301 (2015).
26. M. Y. Han, J. C. Brant, P. Kim, *Phys. Rev. Lett.* **104**, 056801 (2010).
27. S. Jung et al., *Nat. Phys.* **7**, 245–251 (2011).
28. A. G. F. Garcia, M. König, D. Goldhaber-Gordon, K. Todd, *Phys. Rev. B* **87**, 085446 (2013).
29. M. T. Allen et al., *Nat. Phys.* **12**, 128–133 (2016).
30. J. Chae et al., *Nano Lett.* **12**, 1839–1844 (2012).
31. M. J. Zhu et al., *Nat. Commun.* **8**, 14552 (2017).

Science

Imaging resonant dissipation from individual atomic defects in graphene

Dorri HalbertalMoshe Ben ShalomAviram UriKousik BaganiAlexander Y. MeltzerIdo MarcusYuri MyasoedovJohn BirkbeckLeonid S. LevitovAndre K. GeimEli Zeldov

Watching electrons lose steam in graphene

Although graphene can be fabricated to be extremely clean, it still has a nonzero electrical resistance. Resistance is associated with turning electrons' energy into heat, but how exactly does this happen? Halbertal *et al.* used a tiny scanning temperature probe based on a superconducting quantum interference device to investigate this problem. As the current flowed through a square-shaped sample of graphene, electrons lost energy predominantly in the vicinity of atomic-scale defects, which were few and far between in the bulk but much more common on the edges of the sample.

Science, this issue p. 1303

View the article online
https://www.science.org/doi/10.1126/science.aan0877
Permissions
https://www.science.org/help/reprints-and-permissions

Use of this article is subject to the Terms of service